Budapest University of Technology and Economics
Department of Broadband Infocommunications and Electromagnetic Theory

Investigation of Near-field Radiated Power: Modeling, Validation and its Reduction Methods

Summary

Bálint Péter Horváth

Supervisor:
Dr. Péter Horváth

Budapest, 2018

Introduction

Commercial electronic devices have to comply with specific standards to ensure they are not causing any harm in their neighborhood. Besides common EMC (electromagnetic compatibility) and EMI (electromagnetic interference) investigations, portable wireless devices (PWD) are also subject to SAR (specific absorption rate) measurements. (Note that in this work PWD refers to a hand-held, wearable or any other wireless communication devices that may operate in close proximity of the human body.) Such international standards are IEEE C95 [1] and IEC 61000 [2] for EMC/EMI. The exposure limits are defined by ICNIRP [3] and IEEE 1528 [4] and IEC CISPR 16 [5] for SAR. These standards thoroughly describe the measurement procedures required for assessing device compliance. However, since the number of PWDs is growing rapidly, the number of antenna elements per device and the operating frequency of wireless communications increase, the compliance measurements become more and more involved and costly. Furthermore, the higher the frequency, the more the SAR evaluation becomes problematic. The main reasons are that the size of E-field probes become comparable with the wavelength, and because of the skin effect, standard SAR measurements are hard to perform.

A recent approach to overcome these difficulties is to substitute specific measurements with numerical electromagnetic simulations. In fact, standardization is in progress jointly by IEC and IEEE to define procedures for the use of the FDTD (finite difference time domain) and the FE (finite element) methods for electromagnetic compliance evaluation [6] [7]. However, PWDs usually have very complex structures, their geometry often involving extreme aspect ratios. Therefore, the near-field validation of their numerical models is inevitable [8]. This raises the need for affordable numerical validation techniques which can aid the design procedure of such devices.

The power emitted by PWDs (and thus that absorbed by the human tissue) is also strongly dependent on the transmitted waveform. Because its many advantageous properties such as high data rate, tolerance against multipath fading, spectral efficiency, etc., many state-of-art wireless communications standards (WiFi, LTE, DVB-T2, HSDPA, etc.) use multicarrier modulation schemes in the physical layer. Although current standards favor OFDM (orthogonal frequency division multiplexing) as the multicarrier waveform, there are multiple candidates to choose from when it comes to the next generation (5G) mobile and cognitive radio communications [9] [10] [11]. The strengths and weaknesses from an engineering point-of-view vary among these schemes. However, multicarrier waveforms share a common disadvantage, namely high PAPR (peak-to-average power ratio) [12] [13].

High PAPR results in eventual high power transmission and thus prohibits the efficient utilization of power amplifiers. Since OFDM became so wide-spread, there are various methods to reduce its PAPR [14] [15]. Some standards, e.g., the DVB-T2 already includes specific PAPR reduction methods [16]. Nevertheless, when considering the final candidate for the 5G physical layer waveforms, the PAPR and

its reduction possibilities have to be taken into account.

Research goals

One principal objective of the thesis is to present an alternative numerical model validation method of PWDs to the current E-field measurement based approach. As the numerical model validation of radio frequency devices is in an initial stage, the accuracy of a new approach must be comparable to that of the state-of-the-art E-field based technique. As the E-field approach is based on point values of the measured and simulated electric field vectors, the most reassuring way to compare the validation methods is on a point-by-point basis.

There is an ongoing demand for efficient and real-time applicable PAPR reduction schemes. While fundamentally new concepts are getting harder to come up with, even minor modifications to existing methods can have a significant impact on the overall performance of existing schemes. Therefore, an aim is to develop an alteration of the tone reservation scheme used in OFDM systems to improve its PAPR reduction performance.

The limits of PAPR reduction capabilities of FBMC systems are still open question. It is questionable whether the same amount of PAPR reduction is possible with FBMC as with other multicarrier waveforms. The main reason for this is the inherently overlapping nature of FBMC symbols, whereas the symbols of other multicarrier waveforms such as OFDM are orthogonal to each other. Therefore, this thesis aims to investigate the theoretical achievable of specific PAPR reduction methods in FBMC systems.

Research approaches

In my research, I combined analytic and simulation approaches. Where possible the problem formulation is stated analytically. The evaluation is either performed by simulations, or by measurements.

For the numerical model validation, I used analytic approaches to prove equivalence of the proposed validation method with the E-field based technique. To evaluate the underlying impedance change formula, I performed simulations with computational electromagnetic tools and conducted vector network analyzer (VNA) measurements.

For the $\vec{E}^2$ field reconstruction technique, is derived based on the Born approximation. For evaluation, I used the E field results calculated by computational electromagnetic tools. The program performing deconvolution and regularization was developed by myself.

The PAPR problem formulation of the OFDM and FBMC optimization was based on convex optimization theory. To obtain optimal results for the PAPR of OFDM and FBMC symbols, I developed a program which included the use of the

MOSEK 7 convex optimization tool. The tool was only used to solve the quadratic constrained quadratic program (QCQP) of the data generated and evaluated by the proprietary code.

The simulation of the proposed PAPR reduction algorithm for OFDM systems was developed from scratch.

New scientific results

Thesis 1: Numerical model validation method for portable wireless devices [S1][S2]

Validation of the numerical model of devices is based on a quantity that is measured and computed with a computational electromagnetic tool, respectively. Current approaches compare measured and computed values of the E field for evaluation. In my thesis, I introduce an impedance-change based method. For this, two configurations shown in Figure 1 are assumed. Subscripts 1 and 2 are used to denote the electric, $\vec{E}$, and magnetic, $\vec{H}$, field components and material parameters associated with configurations 1 and 2, respectively.

In both configurations, radiating elements made of conductors are embedded in non-uniform linear materials. In most cases, the radiating element is an antenna. For the sake of simplicity, I will subsequently refer to this radiating element as an antenna. The outer boundaries of the investigated volume, Ω_0, are far from the antenna and from the region where the dielectric permittivity, magnetic permeability, or conductivity differs from the ones of the vacuum, ε_0, μ_0, and $\sigma = 0$, respectively.

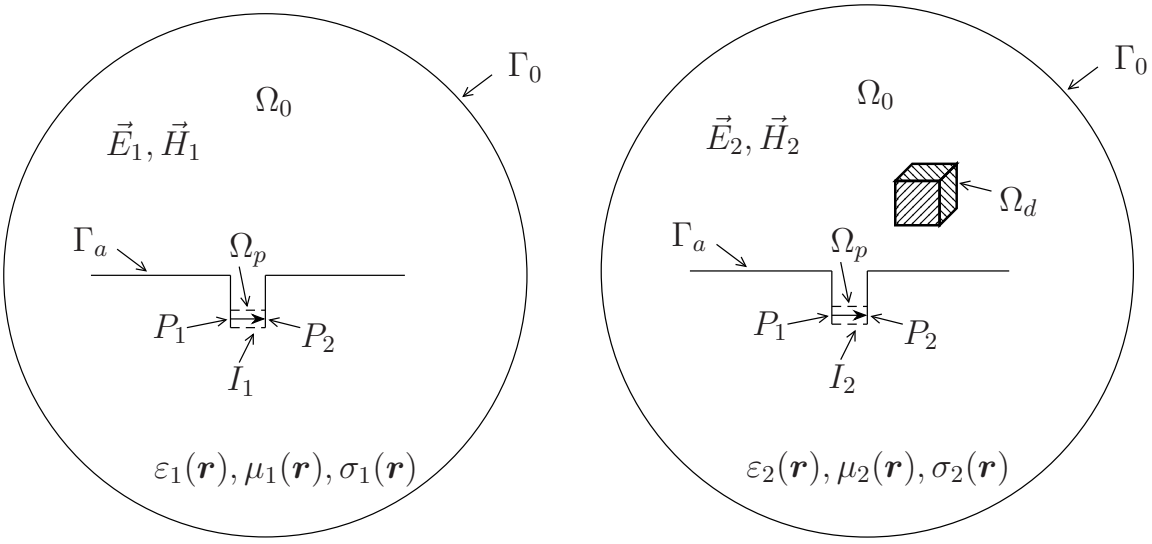

(a) Configuration 1 (without control object) (b) Configuration 2 (with control object)

Figure 1: The investigated configurations

In other words, Ω_0 extends well into the free space. The metallic components of the antenna are considered to be excluded from Ω_0. The surface of the antenna, Γ_a, is an electric wall (the tangential component of $\vec{E}$ is zero on Γ_a) as the conductor forming it is assumed to be PEC (perfect electric conductor). The outer boundary of Ω_0 is denoted Γ_0.

The antenna feed consists of an impressed current filament I_1 (in case of Configuration 1) or I_2 (in case of Configuration 2) flowing between the two terminals, P_1 and P_2 of it. This can be assumed as a lumped element model of a feeding port. The volume, Ω_p is the very close vicinity of the current filament that may represent the volume of a lumped port, which is frequently used in numerical simulations.

The two configurations are almost identical, there are only two exceptions: (i) the feeding currents of the antennas are I_1 and, I_2, respectively, and (ii) the material properties of volume Ω_d are different for the two cases:

$$\begin{array}{llll} \varepsilon_2(\boldsymbol{r}) = \varepsilon_1(\boldsymbol{r}), & \mu_2(\boldsymbol{r}) = \mu_1(\boldsymbol{r}), & \sigma_2(\boldsymbol{r}) = \sigma_1(\boldsymbol{r}), & \boldsymbol{r} \notin \Omega_d, \\ \varepsilon_2(\boldsymbol{r}) \neq \varepsilon_1(\boldsymbol{r}), & \mu_2(\boldsymbol{r}) \neq \mu_1(\boldsymbol{r}), & \sigma_2(\boldsymbol{r}) \neq \sigma_1(\boldsymbol{r}), & \boldsymbol{r} \in \Omega_d. \end{array} \tag{1}$$

From the model conditions, one can derive the impedance change formula

$$\Delta Z = -\frac{1}{I_1 I_2} \int_{\Omega_d} j\omega \left(\varepsilon_2 - \varepsilon_1\right) \vec{E}_1 \cdot \vec{E}_2 \, d\Omega. \tag{2}$$

The formula quantifies the impedance change caused by placing the control object in the near-field of the antenna.

I have proved that the computational electromagnetic model of portable wireless devices can be validated based on one-port characteristic changes caused by a control object placed in the near-field of the antenna.

- **I have proved that the precision of the impedance change scaled with a constant gives an upper bound on the precision of the electric field. Thus, the validation based on the impedance change is equivalent to the electric field based validation.**
- **I have experimentally proved the validity of the presented, reciprocity based impedance change formula. I proved the formula to be applicable by measurement and numerical results of placing a control object in the near-field of the antenna. The results obtained by measurement and calculations made by a computational electromagnetic software are in good agreement.**

The numerical validation of devices is based on the comparison of a quantity that is computed with an electromagnetic solver and measured in the reality. Thus, I have proved the applicability of the impedance change formula in . For the evaluation I designed and manufactured a 1 GHz printed inverted F antenna (PIFA). A 13 mm $\times$ 13 mm $\times$ 13 mm cube with dielectric constant $\varepsilon = 3$ was used as a controll

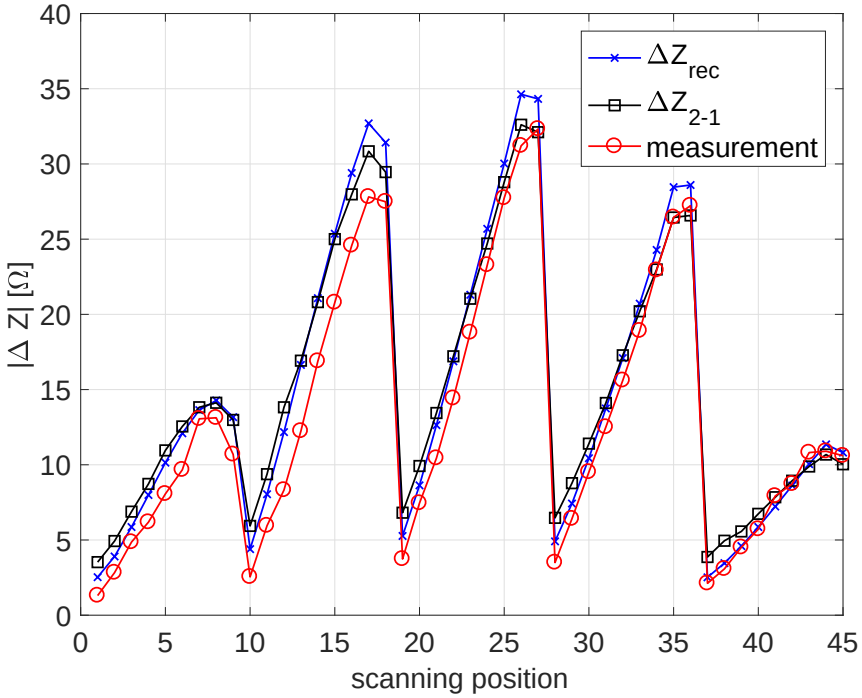

Figure 2: Simulated and measured impedance change of a 1 GHz PIFA antenna in persence of a contol object

object. The cube was placed at 45 five different positions on a scanning grid in the near-field of the antenna. I have used two different type of electromagnetic computation tools to calculate the left- and right-hand side of eq. . I have measured the impedance change of the manufactured antenna with a vector network analyzer. The results of the simulations and measurements are shown in Figure 2. ΔZ_{rec} and ΔZ_{2-1} denotes the right- and left-hand side of the equation, respectively. One can see that both simulation and measurement results are in good agreement with eachother. Thus, the impedance change formula is applicable.

For the validation of the numerical models of DUTs (device under test), the relative error of the impedance change has to be smaller than a prescribed error tolerance δ, that is,

$$\left|\Delta Z' - \widehat{\Delta Z}'\right| < \delta, \tag{3}$$

where the normalized impedance changes are $\Delta Z' = \Delta Z/|Z_1|$ and $\widehat{\Delta Z}' = \widehat{\Delta Z}/|Z_1|$, and Z_1 is the input impedance without the control object present. Quantities with the hat denote exact values while quantities without the hat denote simulated values (i.e., those obtained from the computational electromagnetics tool) One can also introduce the absolute and normalized field errors

$$\vec{e}_1 = \vec{E}_1 - \widehat{\vec{E}}_1, \qquad \vec{e}_2 = \vec{E}_2 - \widehat{\vec{E}}_2, \tag{4}$$

$$\vec{e}_1' = \frac{\vec{e}_1}{E_W} \quad \text{and} \quad \widehat{\vec{E}}_2' = \frac{\widehat{\vec{E}}_2}{E_W}, \tag{5}$$

where the normalization factor is defined as

$$E_W^2 = \frac{1}{\Omega_d} \int_{\Omega_d} \vec{E}_1 \cdot \vec{E}_1^* \, d\nu \tag{6}$$

Following the derivation in the thesis, one can arrive at the inequality

$$\left| \frac{1}{\Omega_d} \int_{\Omega_d} \vec{e}_1' \cdot \widehat{\vec{E}}_2' \, d\nu \right| < \frac{P_A}{\Delta Q_{\Omega_d}} \delta, \tag{7}$$

where $P_A = \frac{1}{2} I^2 |Z_1|$ is the absolute value of the complex input power and $\Delta Q_{\Omega_d} = \omega |\varepsilon_2 - \varepsilon_1| E_W^2 \Omega_d$ is a normalization constant having the physical meaning of the zeroth-order approximation of the reactive power change in the control object due to the presence of the control object. Since the relative error $\vec{e}_1'$ in (7) is tested by a smooth and bounded function $\widehat{\vec{E}}_2'$, (7) implies that the error in field values are limited by the error tolerance δ multiplied by the constant $P_A / \Delta Q_{\Omega_d}$.

Thesis 2: Reconstruction of $\vec{E}^2$ field from impedance change values [S3]

The validation method described in Thesis 1 is proved to be equivalent to the E-field based approach. However, the impedance change formula is an integral quantity, as opposed to the E field values which are point values. Direct comparison of the two techniques would be reassuring. In the following, I show that this is achievable by reconstruction of the $\vec{E}^2$ field. The quantity of $\vec{E}^2$ is closely related to the E field, and also reconstructable from the impedance change values.

I have proven that the $\vec{E}^2$ of an antenna is reconstructable from the impedance change values obtained from placing a control object on a scanning grid in the near-field of an antenna. The reconstruction is possible from the impedance change values using deconvolution if the Born approximation holds for the impedance change formula.

- **I have demonstrated the reconstruction method by numerical simulations using two different antennas**
- **I have shown that the error of the $\vec{E}^2$ field obtained using deconvolution can be significantly reduced if numerical regularization (i.e., truncation or Tikhonov regularization) is applied to the convolution matrix.**

Based on the first-order Born approximation (BA), $\vec{E}_2$ in () can be approximated by $\vec{E}_1$ if the permittivity of volume Ω_d in Configuration 2 is close to the permittivity of Ω_d in the case of Configuration 1. For this situation, one can write:

$$\Delta Z \approx -\frac{1}{I_1 I_2} \int_{\Omega_d} j\omega \left(\varepsilon_2 - \varepsilon_1\right) \vec{E}_1 \cdot \vec{E}_1 \, d\Omega. \tag{8}$$

For an arbitrary control object position $\boldsymbol{r}_d$, one can express the spatial function of the impedance change formula with the BA as

$$\Delta Z\left(\boldsymbol{r}_d\right) = -\frac{j\omega}{I^2} \left(\varepsilon_2 - \varepsilon_1\right) \int\limits_{\Omega_0} p(\boldsymbol{r}_d - \boldsymbol{r}) \vec{E}_1^2(\boldsymbol{r}) \, d\boldsymbol{r}. \tag{9}$$

Notice that (9) is a convolution integral, where $p(\boldsymbol{r})$ is the convolution kernel associated with the control object.

Due to practical reasons detailed in the thesis, the metric

$$E_{1,s}^2(x,y) = \frac{1}{H} \int\limits_{z=z_0}^{z_0+H} \vec{E}_1^2(x,y,z) \, dz \tag{10}$$

is introduced, where z_0 is the distance between the DUT and the control object and H is the height of the control object. Eventually a 2D convolution can be

formulated in one or more arbitrarily chosen $x-y$ planes as

$$\Delta Z\left(x_s, y_s\right) = -\frac{j\omega}{I^2}\left(\varepsilon_2 - \varepsilon_1\right) \int_{x=-\infty}^{\infty} \int_{y=-\infty}^{\infty} P(x_s - x, y_s - y) E_{1,s}^2(x, y)\, dx\, dy, \quad (11)$$

In the thesis I derive, that the convolution and deconvolution can be formulated with simple matrix operations as

$$\boldsymbol{z_B} = C\hat{\boldsymbol{P}}\boldsymbol{e}, \quad (12)$$

$$\text{and} \qquad \boldsymbol{e} = \frac{1}{C}\boldsymbol{z_B}\hat{\boldsymbol{P}}^{-1}, \quad (13)$$

where $C = -\frac{j\omega}{I^2 NM}\left(\varepsilon_2 - \varepsilon_1\right)$, $\hat{\boldsymbol{P}}$ holds the elements $\hat{P}(n,m)$, the discretized convolution kernel, $\boldsymbol{e}$ and $\boldsymbol{z_B}$ are vectors which contain the discretized values of $E_{1,s}^2(n,m)$ and $\Delta Z(n,m)$ in lexicographical order, respectively. Note that (12) is essentially the discretized form of (9).

To quantify the quality of reconstruction two error metrics are defined:

$$\mathrm{MSE}_{\mathrm{mean}} = 100 \frac{\mathrm{mean}\left\{\left|\hat{E}_{1,s}^2(n,m) - \hat{E}_{1,r}^2(n,m)\right|^2\right\}}{\mathrm{mean}\left\{\left|\hat{E}_{1,s}^2(n,m)\right|^2\right\}} \left[\%\right], \quad (14)$$

$$\mathrm{MSE}_{\mathrm{max}} = 100 \frac{\mathrm{mean}\left\{\left|\hat{E}_{1,s}^2(n,m) - \hat{E}_{1,r}^2(n,m)\right|^2\right\}}{\max\left\{\left|\hat{E}_{1,s}^2(n,m)\right|^2\right\}} \left[\%\right], \quad (15)$$

where $\hat{E}_{1,s}^2(n,m)$ is (10) calculated using a computational electromagnetic tool and $\hat{E}_{1,r}^2(n,m)2$ is the result of the deconvolution based resconstruction.

In the thesis, I demonstrate the reconstruction method through numerical simulations using two different antennas, a 1 GHz printed inverted F (PIFA) and a 1.8 GHz printed monopole. The use of deconvolution directly results in intolerable errors in the reconstructed field. However, applying numerical regularization (i.e., truncation or Tikhonov regularization) to the convolution matrix can reduce these errors significantly. In Figure 3a and the $\hat{E}_{1,s}^2(n,m)$ of the PIFA calculated with the CST [17] Microwave Studio is shown. The $\hat{E}_{1,r}^2(n,m)2$ field reconstructed from the impedance change values using deconvolution directly is shown in Figure 3b. The reconstruction results obtained using truncation and Tikhonov regularization are shown in Figures 4a and 4b, respectively.

A benefit of regularization is that it makes the reconstruction method robust against measurement noise. I investigated the case where white Gaussian noise is added to the impedance change values $\boldsymbol{z_B}$. Figure 5a and 5b shows the error metrics (15) and (14) versus the signal to noise ratio (SNR) of $\boldsymbol{z_B}$ for the PIFA and monopole, respectively.

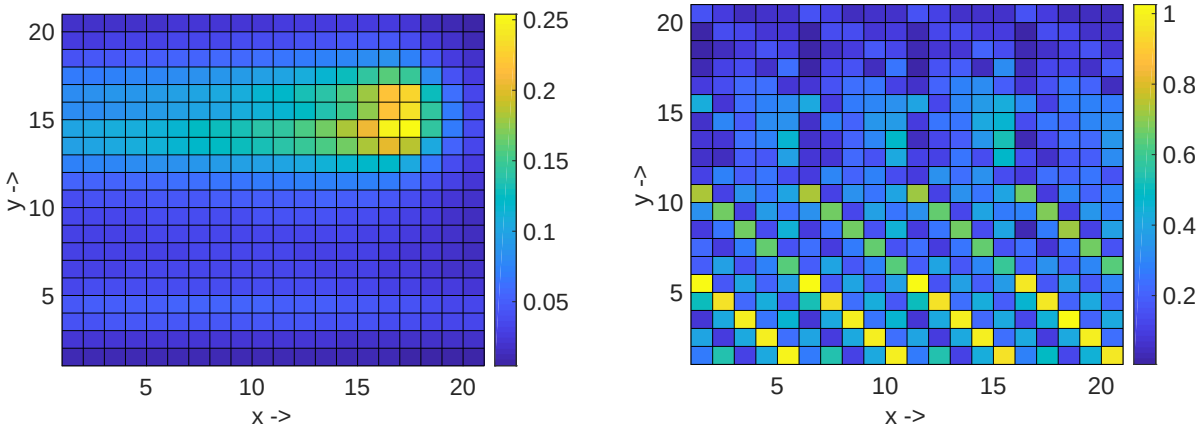

(a) $\left|\hat{E}^2_{1,s}(n,m)\right|$ of 1 GHz PIFA

(b) Deconvolved $\left|\hat{E}^2_{1,r}(n,m)\right|$ from $\Delta\hat{Z}(n,m)$ without regularization

Figure 3: Original and reconstructed field of PIFA

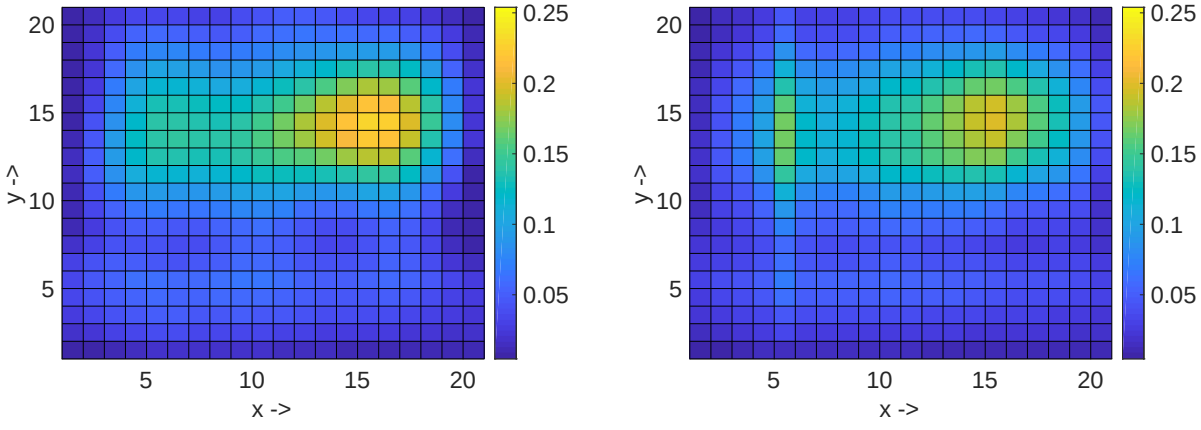

(a) Calculated using truncated convolution matrix from $\Delta\hat{Z}(n,m)$

(b) Calculated using Tikhonov regularized convolution matrix from $\Delta\hat{Z}(n,m)$

Figure 4: Reconstructed $\left|\hat{E}^2_{1,r}(n,m)\right|$ for PIFA

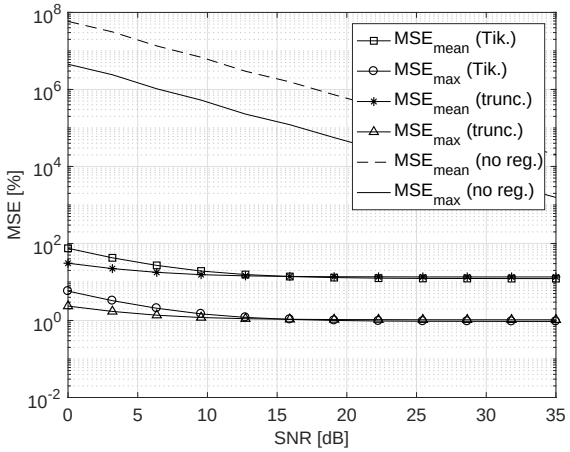

(a) MSE of reconstructed field versus SNR for 1 GHz PIFA

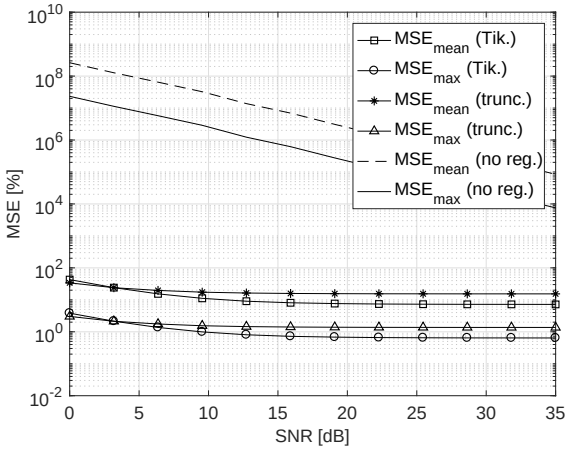

(b) MSE of reconstructed field versus SNR for 1.8 GHz monopole

Figure 5: MSE of reconstructed field versus SNR for two example antennas

Thesis 3: PAPR reduction capabilities in FBMC systems [S4][S5]

The PAPR reduction of multicarrier signals can be formulated as an optimization problem. If convexity of the problem is proven, one can find the unique optimal solution. One can formulate different PAPR reduction methods as constraints on the optimization problem. Because of the inherent overlapping nature of FBMC symbols, it is questionable whether the same rate of PAPR reduction is possible with FBMC as with OFDM.

I have proved that the achievable PAPR reduction with tone reservation (TR), active constellation extension (ACE) and their joint use is similar with OFDM and FBMC modulation.

- **I have formulated and solved the QCQP optimization problem for the PAPR reduction of OFDM and FBMC signals. I have used the constraints of the TR, ACE, and their joint application to reduce the PAPR. The problem formulation includes the number of symbols within an FBMC frame as a parameter which is essential due to the overlapping nature of FBMC symbols.**
- **I have solved the QCQP optimization problem for FBMC and OFDM. The evaluation of the PAPR reduction potential of the TR, ACE, and their joint use is based on the CCDF of the PAPR after solving the problem for a sufficiently large set of symbols with the presented modulation parameters.**

Let $\boldsymbol{x}$ denote the multicarrier modulation signal (OFDM or FBMC). The PAPR of an OFDM symbol is calculated as

$$\mathrm{PAPR}_1 = 10\log_{10}\left(\frac{\max\limits_{0\le k\le NV-1}\left\{|x_k|^2\right\}}{\frac{1}{NV}\sum\limits_{k=0}^{NV-1}|x_k|^2}\right), \tag{16}$$

where N is the number of subcarriers and V denotes the oversampling ratio. For FBMC signals the PAPR is defiend as

$$\mathrm{PAPR}_2 = 10\log_{10}\left(\frac{\max\limits_{mNV\le k\le (m+1)NV-1}\left\{|x_k|^2\right\}}{\frac{1}{NV}\sum\limits_{k=mNV}^{(m+1)NV-1}|x_k|^2}\right), \tag{17}$$

$$K \le m \le M-K-1,$$

where K is the overlapping factor, and M is the number of FBMC symbols in a frame.

Adding the "correction term" $\boldsymbol{y}$ to the original signal and minimizing the instantaneous power of the oversampled complex baseband signal E, the general problem formulation becomes

$$\begin{gathered}\text{minimize } E \qquad \text{subject to} \\ |x_k+y_k|^2 \le E,\ 0\ \le k\ \le T-1,\end{gathered} \tag{18}$$

where T is the length of a frame. The various PAPR reduction methods differ in the constraints they pose on $\boldsymbol{y}$.

Let $\boldsymbol{F^{-1}}$ denote the $NV \times N$ IDFT matrix. Then OFDM signal synthesis can be expressed using matrix operations as $\boldsymbol{x} = \boldsymbol{F^{-1}s}$, where $\boldsymbol{s}$ denotes the frequency domain symbols. Using this notation, the optimization problem for PAPR reduction to a single OFDM symbol can be formulated based on [18]:

$$\begin{gathered}\text{minimize } E \\ \text{subject to} \\ \begin{bmatrix}\boldsymbol{x} & \boldsymbol{F^{-1}}\end{bmatrix}\begin{bmatrix}\mathbf{1}\\ \boldsymbol{t}\end{bmatrix} = \boldsymbol{a} \\ E \ge |a_k|^2,\end{gathered} \tag{19}$$

where $\boldsymbol{a}$ is an auxiliary variable to express the amplitude of the signal. The instantaneous magnitude $|a_k|^2$ is upper bounded by E which is minimized.

In the thesis I derive the formulation of the PAPR optimization problem for FBMC in a similar form. It is shown in my thesis that one can express the synthesis of an FBMC frame as

$$\boldsymbol{x} = \boldsymbol{H_{F1}}\boldsymbol{t}_{re} + \boldsymbol{H_{F2}}\boldsymbol{t}_{im}, \tag{20}$$

where $\boldsymbol{t}\boldsymbol{t}_{re} + j\boldsymbol{t}_{im}$ denotes the frequency domain symbols for the entire frame, i.e., for M successive symbols, $\boldsymbol{H_{F1}}$ and $\boldsymbol{H_{F2}}$ are the FBMC synthesis matrices. Then the optimization problem for FBMC becomes:

$$\begin{gathered} \text{minimize } E \\ \text{subject to} \\ \begin{bmatrix} \boldsymbol{x} & \boldsymbol{H_{F1}} & \boldsymbol{H_{F2}} \end{bmatrix} \begin{bmatrix} \mathbf{1} \\ \boldsymbol{t}_{re} \\ \boldsymbol{t}_{im} \end{bmatrix} = \boldsymbol{a} \\ E \geq |a_k|^2. \end{gathered} \tag{21}$$

Both OFDM and FBMC optimization problems are indeed a QCQPs. In my thesis, I show that the problem is convex and thus, a unique solution exists. I used proprietary code in combination with the MOSEK 7 [19] optimization tool to obtain the optimal results. I my thesis, I have performed simulations with parameters shown in Table 1. The result of PAPR reduction with the TR, ACE, and their joint use is shown in Figure 6 and Figure 7 for OFDM and FBMC with $M = 8$ symbols per frame, respectively. The modulation alphabet is 16QAM for both schemes. All other parameters are set according to Table 1. The CCDF curves reveal that, if computational complexity is not a concern, the PAPR reduction capability of TR, ACE and their joint application is similar in OFDM and FBMC systems.

Table 1: Simulation parameters

Parameter	FBMC	OFDM
no. of subcarriers [N]	64	64
frame size [M]	8,12	1
overlapping factor [K]	4	0
no. of reserved tones [N_{PRC}]	5	5
oversampling rate [V]	4	4
no. of realizations	1000	1000
modulation alphabet	QPSK, 16QAM	QPSK, 16QAM

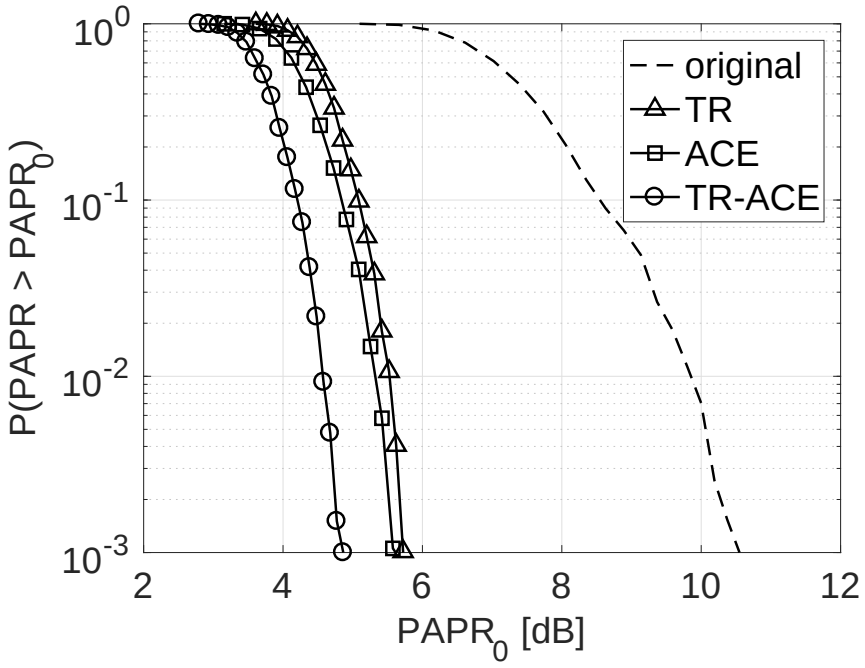

Figure 6: CCDF of PAPR for original and PAPR reduced OFDM signal

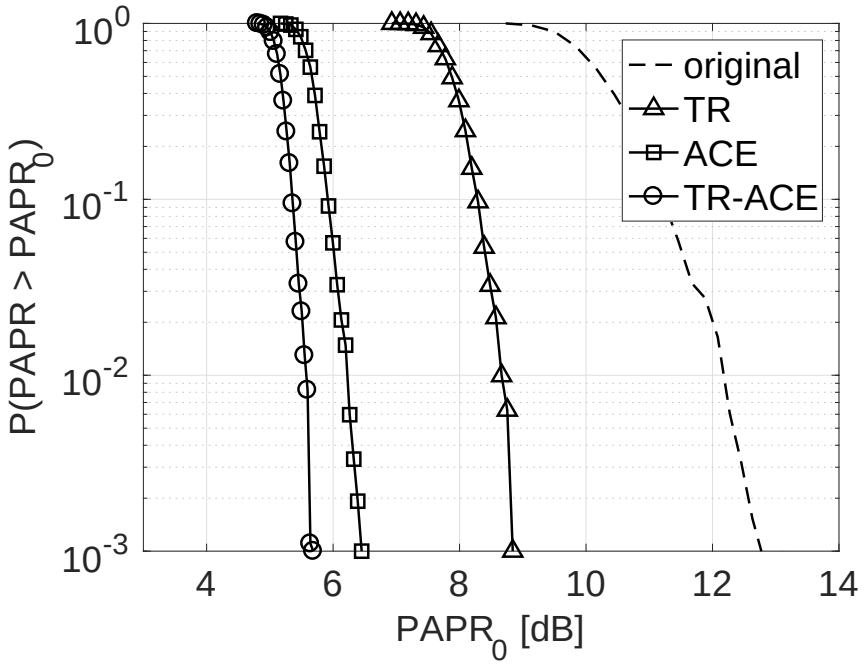

Figure 7: CCDF of PAPR for original and PAPR reduced FBMC signal, $M = 8$ symbols per frame

Thesis 4: Improved PAPR reduction method for OFDM systems [S6]

The optimal solution of the PAPR problem is attractive, however solving the QCQP in real-time might not be possible. Thus, computationally efficient suboptimal algorithms are developed that can be applied in practice. Such methods are the kernel-based (TR-K) [20] [21] and clipping-based (TR-C) [22] [23] tone reservation schemes.

I have proved that the PAPR reduction capability of the TR-C and TR-K method can be improved in OFDM systems if the clipping ratio is adjusted iteratively.

- **I have shown that the PAPR reduction capability of the TR-C and TR-K techniques depends on the CR. I have proposed two methods to determine the iteration dependent CR trajectory, the "globally" and the "locally" improved CR.**
- **I have proved that when the globally and locally improved CR is applied, then the PAPR reduction capability of the TR-C and TR-K is enhanced. The evaluation of the PAPR reduction potential is based on the CCDF of the PAPR after solving the problem with the compared methods for a sufficiently large set of symbols with the presented modulation parameters.**

Both TR-K and TR-C methods can be performed iteratively and they have the clipping ratio (CR) as a parameter:

$$\mathrm{CR}^i_{\mathrm{dB}} = 10\log_{10}\left(\frac{\left(A^i_{\max}\right)^2}{\frac{1}{NV}\sum\limits_k |x_k|^2}\right), \tag{22}$$

where $A^i_{\max}$ is the clipping amplitude in the i^{th} iteration.

In the TR-K scheme the output signal is modified according to a predefined kernel function. The kernel function is scaled with α and circularly shifted with m samples in every iteration.

$$\boldsymbol{x}^{i+1} = \boldsymbol{x}^i - \alpha^i \boldsymbol{r}(m^i), \tag{23}$$

$$\alpha^i = \frac{x^i_{m^i}}{A^i}(A^i - A_{\max}), \tag{24}$$

where $\boldsymbol{r}$ is the kernel function. The sum of scaled and shifted functions is added to the original signal. The transmit signal after the i^{th} iteration is

$$\boldsymbol{x}^i = \boldsymbol{x} + \sum_{g=1}^{i} \alpha^g \boldsymbol{r}(m^g). \tag{25}$$

In case of the TR-C scheme, the signal is clipped in each iteration as

$$\bar{x}_k = \begin{cases} x_k, & \text{if } x_k < A^i_{\max} \\ A^i_{\max}\, e^{j\varphi(x_k)}, & \text{if } x_k > A^i_{\max} \end{cases}, \tag{26}$$

where $\bar{x}_k$ is the clipped signal and $\varphi(x_k)$ is the phase of the signal. To obtain the PAPR reduced signal, the clipped signal is further manipulated in the way described in the thesis.

Former methods did not exploit the feature that the CR can be modified in every iteration. In my thesis, I have presented two methods, the "globally" and "locally" improved CR to find a beneficial CR trajectory. I have evaluated the performance improvement of the PAPR reduction methods through simulations with parameters shown in Table 2. In Figure 8 the CCDF function of the PAPR is shown when the globally and locally improved CR is used. The Figure also shows the results when the CR is not adjusted during iterations. It is clear, that for the TR-C algorithm both the globally and the locally improved CR is advantageous. On the other hand for the TR-K scheme, only the results of the locally improved CR are significantly better.

Parameter	value
modulation	OFDM
no. of subcarriers [N]	2048
no. of reserved tones [N_{PRC}]	18
position of peak reduction carriers (PRC)	113, 124, 262, 467, 479, 727, 803, 862, 910, 946, 980, 1201, 1322, 1342, 1396, 1397, 1562, 1565
maximal allowed PRC amplitude	5
number of symbols	15000
modulation alphabet	16-QAM
oversampling rate [V]	4
μ for TR-C	-282

Table 2: Simulation parameters of the TR-K and TR-C methods

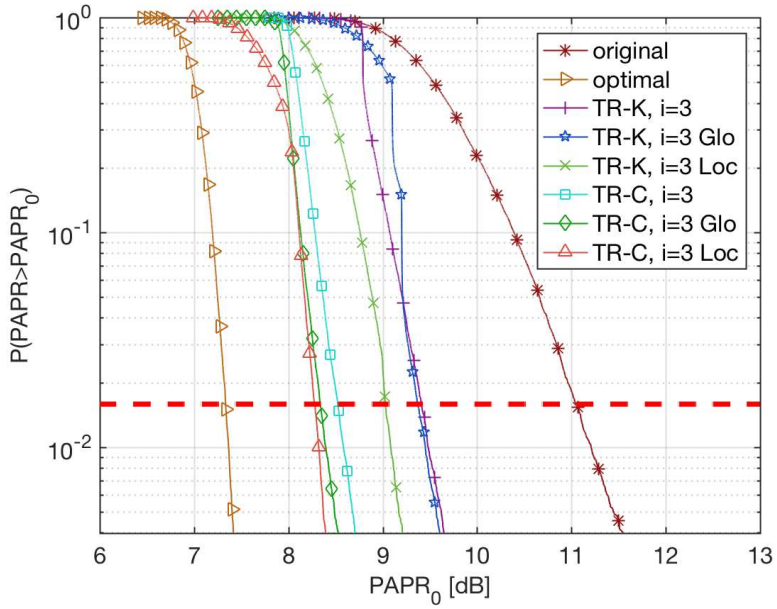

Figure 8: CCDF comparison of the constant, locally and globally improved CR with TR-K and TR-C algorithms

Outlook

A possible application to numerical validation and near-field reconstruction method related to Thesis 1. and 2. is pre-compliance with standards that need numerical validation such as [24]. However, as the technique becomes more mature, it will potentially become an alternative to the E-field based approach even in standards. For this to happen, further benchmark measurements and comparison with conventional methods are needed.

Future work regarding Thesis 3. is to find algorithms that can approach the PAPR reduction capability of the theoretical results in real-time. With the help of the presented problem formulation and solution, one can analyze the optimal result which can motivate the development of new methods for FBMC.

The results presented in Thesis 4. can be applied in standards where the TR reduction scheme is allowed. An example of such a system is DVB-T2 [16]. Furthermore, based on the presented method one can find an improved CR trajectory for other clipping based PAPR reduction methods such as active constellation extension.

References

[1] *IEEE C95 - Safety Levels with respect to human exposure to radio frequency electromagnetic fields*, Institute of Electrical and Electronics Engineers Std., 2005.

[2] *IEC 61000 - Electromagnetic compatibility (EMC)*, International Electrotechnical Commission Std., 2014.

[3] "International commission on non-ionizing radiation protection and others (ICNIRP) statement on the guidelines for limiting exposure to time-varying electric, magnetic, and electromagnetic fields (up to 300 GHz)," *Health physics*, vol. 97, no. 3, pp. 257–258, 2009.

[4] *IEEE 1528 - Recommended Practice for Determining the Peak Spatial-Average Specific Absorption Rate (SAR) in the Human Head from Wireless Communications Devices: Measurement Techniques*, Institute of Electrical and Electronics Engineers Std., 2013.

[5] *IEC CISPR 16 - Specification for radio disturbance and immunity measuring apparatus and methods*, International Electrotechnical Commission Std., 2015.

[6] "IEC/IEEE international standard for determining the peak spatial average specific absorption rate (SAR) in the human body from wireless communications devices, 30 MHz - 6 GHz. part 1: General requirements for using the finite difference time domain (FDTD) method for SAR calculations," *IEEE P62704-1D4*, pp. 1–94, Jan. 2016.

[7] "IEC/IEEE draft international standard for determining the peak spatial-average specific absorption rate (SAR) in the human body from wireless communications devices, 30 MHz - 6 GHz, part 4: General requirements for using the finite-element method for sar calculations and specific requirements for modelling vehicle-mounted antennas and personal wireless devices," *IEC/IEC P62704-4*, 2016.

[8] V. Monebhurrun, X. Cheng, and A. Rojatkar, "CAD mobile phone model calibration using experimental specific absorption rate data," in *Radio and Antenna Days of the Indian Ocean (RADIO), 2015*. IEEE, 2015, pp. 1–2.

[9] F. Schaich and T. Wild, "Waveform contenders for 5G - OFDM vs. FBMC vs. UFMC," in *Communications, Control and Signal Processing (ISCCSP), 2014 6th International Symposium on*. IEEE, 2014, pp. 457–460.

[10] N. Michailow, M. Matthé, I. S. Gaspar, A. N. Caldevilla, L. L. Mendes, A. Festag, and G. Fettweis, "Generalized frequency division multiplexing for 5th generation cellular networks," *IEEE Transactions on Communications*, vol. 62, no. 9, pp. 3045–3061, 2014.

[11] B. Farhang-Boroujeny, "OFDM versus filter bank multicarrier," *IEEE Signal Processing Magazine*, vol. 28, no. 3, pp. 92–112, 2011.

[12] R. Prasad, *OFDM for Wireless Communications Systems*. Artech House, Inc., 2004.

[13] R. Gerzaguet, N. Bartzoudis, L. G. Baltar, V. Berg, J.-B. Doré, D. Kténas, O. Font-Bach, X. Mestre, M. Payaró, M. Färber *et al.*, "The 5G candidate waveform race: a comparison of complexity and performance," *EURASIP Journal on Wireless Communications and Networking*, vol. 2017, no. 1, p. 13, 2017.

[14] S. H. Han and J.-H. Lee, "An overview of peak-to-average power ratio reduction techniques for multicarrier transmission," *IEEE Wireless Communication*, pp. 56–65, Apr. 2005.

[15] P. Foomooljareon and W. Fernando, "PAPR reduction in OFDM systems," *Thammasa Int. J. Sc. Tech.*, vol. 7, no. 3, 2002.

[16] ETSI, *Digital Video Broadcasting (DVB); Frame structure channel coding and modulation for a second generation digital terrestrial television broadcasting system (DVB-T2)*, ETSI EN 302 755 V.1.3.1, Std., Apr. 2012.

[17] "CST microwave studio," 2017. [Online]. Available: www.cst.com

[18] B. Krongold and D. Jones, "PAR reduction in OFDM via active constellation extension," *IEEE Transactions on Broadcasting*, vol. 49, no. 3, pp. 258–268, Sep. 2003.

[19] MOSEK ApS, *The MOSEK optimization toolbox for MATLAB*, 2015.

[20] P. Yu and S. Jin, "A low complexity tone reservation scheme based on time-domain kernel matrix for PAPR reduction in OFDM systems," *IEEE Transactions on Broadcasting*, vol. 61, no. 4, pp. 710–716, Dec 2015.

[21] R. Barsanti and J. Larue, "Peak to average power ratio reduction for digital video broadcast T2," in *Proceedings of IEEE Southeastcon 2011*, Mar. 2011, pp. 117–121.

[22] T. Liu, X. Li, C. Chen, S. Cui, and Y. Liu, "PAPR reduction for 802.16e by clipping and tone reservation based on amplitude scale factor," in *ICPCA/SWS'12, Proceedings of the 2012 International Conference on Pervasive Computing and the Networked World*. Berlin, Heidelberg: Springer-Verlag, 2013, pp. 339–349, ISBN:978-3-642-37014-4.

[23] S. Janaaththanan, C. Kasparis, and B. Evans, "A gradient based algorithm for PAPR reduction of OFDM using tone reservation technique," in *Vehicular Technology Conference, 2008. VTC Spring 2008. IEEE*, May 2008, pp. 2977–2980.

[24] "IEC/IEEE draft international standard - determining the peak spatial-average specific absorption rate (SAR) in the human body from wireless communications devices, 30 MHz - 6 GHz part 3: Specific requirements for using the finite difference time domain (FDTD) method for SAR calculations of mobile phones," *IEC/IEEE P62704-3/D4*, pp. 1–47, Jan. 2017.

Thesis-related own publications

[S1] B. Horváth, Zs. Badics, J. Pávó, and P. Horváth, "Validation of numerical models of portable wireless devices for near-field simulation," *IEEE Transactions on Magnetics*, vol. 53, no. 6, pp. 1–4, 2017.

[S2] B. Horváth, P. Horváth, Zs. Badics, and J. Pávó, "Computational model validation of wireless devices for specific absorption rate evaluation," in *2016 10th European Conference on Antennas and Propagation (EuCAP)*. IEEE, 2016, pp. 1–4.

[S3] B. Horváth, P. Horváth, Z. Badics, and J. Pávó, "Near-field reconstruction for portable wireless devices by deconvolution from input impedance changes," *IET Science, Measurement & Technology*, 2018.

[S4] B. Horváth and P. Horváth, "Establishing lower bounds on the peak-to-average-power ratio in filter bank multicarrier systems," *Infocommunications Journal*, vol. 7, no. 3, pp. 10–16, 2015.

[S5] B. Horváth, Zs. Kollár, and P. Horváth, "Bridging the gap between optimal and suboptimal ACE PAPR reduction scheme for OFDM," in *Radioelektronika, 2014 24th International Conference*. IEEE, 2014, pp. 1–4.

[S6] B. Horváth and B. Botlik, "Optimization of tone reservation-based PAPR reduction for OFDM systems," *Radioengineering*, vol. 26, no. 3, p. 791, 2017.

Other publications

[P1] M. Schmidt, L. Csurgai-Horváth, P. Horváth, B. Horváth, A. Martellucci, and J. R. Castro, "Architectural design of the Q/V band site diversity experiment between Austria and Hungary," in *International Conference on Wireless and Satellite Systems*. Springer, 2017, pp. 184–194.

[P2] B. Horváth and P. Horváth, "Flat spectrum signal synthesis in filter bank multicarrier systems," in *Transparent Optical Networks (ICTON), 2015 17th International Conference on*. IEEE, 2015, pp. 1–4.

[P3] Zs. Kollár, L. Varga, B. Horváth, P. Bakki, and J. Bitó, "Evaluation of clipping based iterative PAPR reduction techniques for FBMC systems," *The Scientific World Journal*, vol. 2014, 2014.

[P4] B. Horváth and P. Bakki, "Implementation of FBMC transmission link using SDR," in *Radioelektronika, 2013 23rd International Conference*. IEEE, 2013, pp. 320–323.